INTERNATIONAL JOURNAL FOR NUMERICAL METHODS IN FLUIDS
Int. J. Numer. Meth. Fluids 2008; **56**:1705–1729
Published online 23 August 2007 in Wiley InterScience (www.interscience.wiley.com). DOI: 10.1002/fld.1575

A numerical method for forced convection in porous and homogeneous fluid domains coupled at interface by stress jump

Xiaobing Chen[1], Peng Yu[1], S. H. Winoto[1] and Hong-Tong Low[2,*,†,‡]

[1]*Department of Mechanical Engineering, National University of Singapore, Singapore 117576, Singapore*
[2]*Division of Bioengineering, National University of Singapore, Singapore 117576, Singapore*

SUMMARY

A numerical method was developed for flows involving an interface between a homogeneous fluid and a porous medium. It is based on the finite volume method with body-fitted and multi-block grids. The Brinkman–Forcheimmer extended model was used to govern the flow in the porous medium region. At its interface, the flow boundary condition imposed is a shear stress jump, which includes the inertial effect, together with a continuity of normal stress. The thermal boundary condition is continuity of temperature and heat flux.

The forced convection through a porous insert over a backward-facing step is investigated. The results are presented with flow configurations for different Darcy numbers, 10^{-2} to 10^{-5}, porosity from 0.2 to 0.8, Reynolds number from 10 to 800, and the ratio of insert length to channel height from 0.1 to 0.3. The heat transfer is improved by using porous insert. To enhance the heat transfer with minimal frictional losses, it is preferable to have a medium length of insert with medium Darcy number, and larger Reynolds number. The interfacial stress jump coefficients β and β_1 were varied from -1 to 1, and within this range the average and local lower-wall Nusselt numbers are not sensitive to the parameters. Copyright © 2007 John Wiley & Sons, Ltd.

Received 2 February 2007; Revised 16 June 2007; Accepted 18 June 2007

KEY WORDS: interfacial boundary condition; porous medium; backward-facing step; forced convection; porous/fluid domains; stress jump

1. INTRODUCTION

It has been demonstrated that the insertion of porous material can enhance the heat transfer with little additional frictional loss. Huang and Vafai [1] studied the flow in a two-dimensional duct

*Correspondence to: Hong-Tong Low, Division of Bioengineering, National University of Singapore, Singapore 117576, Singapore.
†E-mail: mpelowht@nus.edu.sg
‡Associate Professor.

with intermittently placed porous blocks located on one of the walls, and later they imbedded these blocks within the duct walls [2]. Fu *et al*. [3] studied the forced convection in a laminar channel, which has a porous block on one wall.

Heat transfer would be enhanced if the flow has regions of recirculation and its reduction or elimination is highly desirable, as wall temperatures are typically high in these regions. Abu-Hijleh [4] numerically investigated the flow over a backward-facing step with a porous floor segment whose porosity was varied by changing the pressure loss coefficients, and showed that the maximum local Nusselt number was higher. Martin *et al*. [5] numerically investigated the heat transfer enhancement with porous inserts behind the backward-facing step, with high porosity above 0.90 and $Re = 800$. Generally, the porous inserts reduce or eliminate the lower wall recirculation zone, but in some cases the recirculation zone is lengthened if the inserts are short and extremely porous. More recently, Zhang and Zhao [6] solved the same problem using a high-order characteristics upwind finite-volume algorithm. The fluid region was governed by the Navier–Stokes equation and the porous region by the Brinkman–Forchheimer-extended Darcy model. The two equations were unified into one set for both the fluid and porous media regions by introducing a binary parameter which had values one and zero in porous and fluid regions, respectively. Thus, the matching conditions at the interface were automatically satisfied. For such a single-domain approach, the physical values at the interface depend on the type of discretization scheme.

The present paper simulates the forced convection flow over a two-dimensional backward-facing step with a different approach. A two-domain approach is used for the porous and fluid parts in order to allow for various types of interfacial conditions which includes non-continuity of shear stress. The control equations in these two domains are Navier–Stokes equations and Darcy–Brinkman–Forchheimer-extended model for fluid and porous regions, respectively.

The interfacial conditions have to be coupled in solving the equations for the two regions and additional boundary conditions are applied at the interface. Boundary conditions for flow and heat transfer at the porous–fluid interface have been proposed previously and summarized in Tables I and II.

One of the early flow boundary conditions was that of Beavers and Joseph [7] who proposed the slip-boundary condition, in which the interfacial fluid shear was related to the interface fluid velocity and the Darcy flow was assumed in the porous region. The interface condition contained a jump in both stress and velocity. However, a continuity in both velocity and stress was proposed by Neale and Nader [8] as well as Vafai and Kim [9]. The continuity of shear stress was also assumed by Vafai and Thiyagaraja [10] as well as Kim and Choi [11], but there is non-continuity of velocity gradient, which is satisfied by using an effective viscosity for the porous medium region.

The non-continuity of both velocity gradient and shear stress has been developed by Ochoa-Tapia and Whitaker [12, 13]. The development was based on the non-local form of the volume-averaged Stokes' equation. The length-scale constraint was that the radius of the averaging volume is much smaller than the height of the fluid channel. Under these circumstances, the volume-averaged equations in the homogeneous fluid regions are equivalent to the point equations; and the analysis of jump condition is greatly simplified because a single volume-averaged transport equation is valid in both fluid and porous regions. The jump condition joins the Darcy law, with Brinkman's correction, to the Stokes equation. The analysis produced a jump in the stress but not in the velocity. The normal component of jump condition simply reduced to continuity of pressure. The function for the jump coefficient indicates dependence on permeability and porosity and was complex to solve. The coefficient was expected to be of the order 1, and may be either positive or negative. It was noted that the parameter depends on $\sqrt{K}/\delta$, where δ is the thickness of the boundary region.

DOI: 10.1002/fld

Table I. Velocity boundary conditions at interface between porous and fluid domains.

Model	Velocity	Velocity gradient	Reference
1		$\left.\frac{\partial u_x}{\partial y}\right\|_{\text{fluid}} = \frac{\alpha}{\sqrt{K}}(u_x\|_{\text{interface}} - \langle u\rangle_\infty)$	[7]
2	$\langle u\rangle_x\|_{\text{porous}} = u_x\|_{\text{fluid}}$	$\left.\frac{\partial\langle u\rangle_x}{\partial y}\right\|_{\text{porous}} = \left.\frac{\partial u_x}{\partial y}\right\|_{\text{fluid}}$	[8, 9]
3	$\langle u\rangle_x\|_{\text{porous}} = u_x\|_{\text{fluid}}$	$\mu_{\text{eff}}\left.\frac{\partial\langle u\rangle_x}{\partial y}\right\|_{\text{porous}} = \mu\left.\frac{\partial u_x}{\partial y}\right\|_{\text{fluid}}$	[10, 11]
4	$\langle u\rangle_x\|_{\text{porous}} = u_x\|_{\text{fluid}}$	$\frac{\mu}{\varepsilon}\left.\frac{\partial\langle u\rangle_x}{\partial y}\right\|_{\text{porous}} - \mu\left.\frac{\partial u_x}{\partial y}\right\|_{\text{fluid}} = \beta\left.\frac{\mu}{\sqrt{K}}u_x\right\|_{\text{interface}}$	[12–15]
5	$\langle u\rangle_x\|_{\text{porous}} = u_x\|_{\text{fluid}}$	$\frac{\mu}{\varepsilon}\left.\frac{\partial\langle u\rangle_x}{\partial y}\right\|_{\text{porous}} - \mu\left.\frac{\partial u_x}{\partial y}\right\|_{\text{fluid}} = \beta\left.\frac{\mu}{\sqrt{K}}u_x\right\|_{\text{interface}} + \beta_1\rho u_x^2\|_{\text{interface}}$	[16]

Table II. Heat transfer boundary conditions at interface between porous and fluid domains.

Model	Temperature	Temperature gradient	Reference
1	$\langle T\rangle\|_{\text{porous}} = T\|_{\text{fluid}}$	$k_{\text{eff}}\left.\frac{\partial\langle T\rangle}{\partial y}\right\|_{\text{porous}} = k_{\text{f}}\left.\frac{\partial T}{\partial y}\right\|_{\text{fluid}}$	[8, 10, 11, 17–19]
2	$\langle T\rangle\|_{\text{porous}} = T\|_{\text{fluid}}$	$k_{\text{eff}}\left.\frac{\partial\langle T\rangle}{\partial y}\right\|_{\text{porous}} = k_{\text{f}}\left.\frac{\partial T}{\partial y}\right\|_{\text{fluid}} + \phi$	[20]
3	$\left.\frac{\mathrm{d}T}{\mathrm{d}y}\right\|_{\text{fluid}} = \frac{\alpha_T}{\lambda}(T\|_{\text{fluid}} - \langle T\rangle\|_{\text{porous}})$	$k_{\text{eff}}\left.\frac{\partial\langle T\rangle}{\partial y}\right\|_{\text{porous}} = k_{\text{f}}\left.\frac{\partial T}{\partial y}\right\|_{\text{fluid}}$	[21]

Subsequently, Ochoa-Tapia and Whitaker [16] developed another stress jump condition, which includes the inertial effects. Though inertial effects may be negligible in homogeneous regions of channel flow, it is not negligible in the boundary between the porous and fluid regions. Outside the boundary regions, the non-local form of the volume-averaged momentum equation reduces to the Forchheimer equation with Brinkman correction and the Navier–Stokes equation. Two coefficients appear in this jump condition: one is associated with an excess viscous stress and the other is related to an excess inertial stress.

Ochoa-Tapia and Whitaker [16] derived analytical expressions for parameters β and β_1, which indicate their dependence on permeability and porosity. They concluded that these two parameters are both of order 1. Ochoa-Tapia and Whitaker [13] experimentally determined that β varies from $+0.7$ to -1.0 for different materials with permeability varying from 15×10^{-6} to 127×10^{-6} in^2 and average pore size from 0.016 to 0.045 in. There is presently no experimental data for β_1. It is

DOI: 10.1002/fld

not known how much the two parameters may change from one type of interface to another; and it is assumed, in this study, that the changes should be in the same range as those for different types of materials.

The stress jump parameter (associated with an excess viscous stress) was derived by Goyeau *et al*. [14] as an explicit function of the effective properties of a transition layer between the fluid and porous regions. The parameter is also related to the variations of the velocity in the transition layer, which is an unknown in the problem. Recently, Chandesris and Jamet [15] presented a model, in which the shear jump is built on the fluid stress rather than on the effective stress. An explicit function for the stress jump coefficient was obtained which only depends on the characteristics of the porous medium (porosity and permeability) in the transition zone.

Numerical solutions for the coupled viscous and porous flows have been attempted by many researchers [22–26]. Jue [22] simulated vortex shedding behind a porous square cylinder by finite element method. In his study, a general non-Darcy porous media model was applied to describe the flows both inside and outside the cylinder. A harmonic mean was used to treat the sudden change between the fluid and porous medium. Costa *et al.* [24] proposed a control-volume finite element method to simulate the problems of coupled viscous and porous flows. A continuity of both velocity and stress at the interface was assumed and no special or additional procedure was needed to impose the interfacial boundary conditions. Betchen *et al.* [26] developed a finite volume model, also based on continuity of both velocity and stress, but special attention was given to the pressure–velocity coupling at the interface.

Different types of interfacial conditions between a porous medium and a homogeneous fluid have been proposed; and found to have a pronounced effect on the velocity field as shown by Alazmi and Vafai [27]. The one-domain approach has an automatically satisfied continuity of both velocity and stress, which is easier to implement. Nevertheless, the stress jump conditions have been adopted by many researchers.

The implementation of the numerical methodology on the stress jump condition based on Ochoa-Tapia and Whitaker [12, 13] can be found in the work of Silva and de Lemos [23]. Although they proposed that their treatment could be used in a complex geometry, their results were based on finite volume method in an orthogonal Cartesian coordinate system and for the case of fully developed flow. In their study, only the jump in shear stress was included and no special treatment on velocity derivatives was mentioned. However, for flow in general, it is needed to consider how to formulate the velocity derivatives at the interface. Also, for the two-dimensional problem, the normal stress condition is needed to close the sets of equations.

For heat transfer interface conditions, usually continuities of temperature and heat flux are required [8, 10, 11, 17–19]. However, other types of interfacial conditions are also possible. Ochoa-Tapia and Whitaker [20] proposed a jump condition for heat flux to account for its production or consumption at the interface. Another hybrid interfacial condition, continuity of heat flux but non-continuity in temperature, was proposed by Sahraoui and Kaviany [21].

The objective of the present study was to implement a numerical method based on finite volume method to treat the interfacial boundary conditions for both flow and heat transfer. It adopts the stress jump condition given by Ochoa-Tapia and Whitaker [16], which includes the inertial effects. For heat transfer, the continuity of temperature and heat flux is implemented although the present method can also treat other interfacial conditions. The present method extends a previous study by Yu *et al*. [28] who only treated flow interfacial conditions. The present implementation is demonstrated on the flow and forced convection in a backward-facing step with a porous insert. The range of Reynolds number is from 10 to 800, Darcy number from 10^{-2} to 10^{-5}, and porosity

DOI: 10.1002/fld

from 0.2 to 0.8. The stress jump interfacial condition effects on the average Nusselt number are also considered.

2. MATHEMATICAL MODEL

Steady, two-dimensional, laminar and incompressible flow over a backward-facing step is considered here (Figure 1). The porous insert is located after the step. The inlet flow velocity is specified as a parallel flow with a parabolic horizontal component given by $u(y) = 24y(0.5 - y)$ for $0 \leqslant y \leqslant 0.5$. This produces an average inflow velocity of $u_{\mathrm{av}} = 1.0$, which is treated as the reference velocity. The inlet flow and step wall temperature are set to T_{i}; the upper and bottom wall supply a constant heat flux q; and the outlet condition is adiabatic.

The porous medium is considered to be rigid, homogeneous and isotropic; and saturated with the same single-phase fluid as that in the homogeneous fluid region. Considering viscous and inertial effects, the governing equations for porous region based on Darcy–Brinkman–Forchheimer extended model can be expressed as [29, 30]

Continuity equation:

$$\frac{\partial u}{\partial x} + \frac{\partial v}{\partial y} = 0 \tag{1}$$

X-momentum equation:

$$\frac{1}{\varepsilon}\left\{u\frac{\partial}{\partial x}\left(\frac{u}{\varepsilon}\right) + v\frac{\partial}{\partial y}\left(\frac{u}{\varepsilon}\right)\right\} = -\frac{1}{\varepsilon}\frac{\partial}{\partial x}(\varepsilon p_f) - \frac{1}{Da \cdot Re}u - \frac{1.75}{\sqrt{150}}\frac{(u^2+v^2)^{1/2}}{\sqrt{Da}}\frac{u}{\varepsilon^{3/2}} + \frac{1}{\varepsilon \cdot Re}\left(\frac{\partial^2 u}{\partial x^2} + \frac{\partial^2 u}{\partial y^2}\right) \tag{2}$$

Y-momentum equation:

$$\frac{1}{\varepsilon}\left\{u\frac{\partial}{\partial x}\left(\frac{v}{\varepsilon}\right) + v\frac{\partial}{\partial y}\left(\frac{v}{\varepsilon}\right)\right\} = -\frac{1}{\varepsilon}\frac{\partial}{\partial y}(\varepsilon p_f) - \frac{1}{Da \cdot Re}v - \frac{1.75}{\sqrt{150}}\frac{(u^2+v^2)^{1/2}}{\sqrt{Da}}\frac{v}{\varepsilon^{3/2}} + \frac{1}{\varepsilon \cdot Re}\left(\frac{\partial^2 v}{\partial x^2} + \frac{\partial^2 v}{\partial y^2}\right) \tag{3}$$

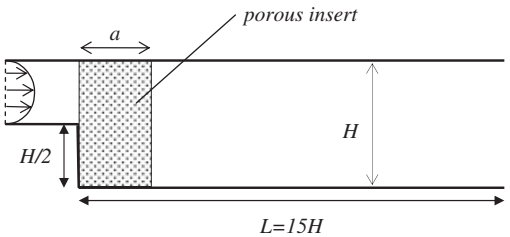

Figure 1. Schematic of the flow model.

DOI: 10.1002/fld

Energy equation:

$$u\frac{\partial T}{\partial x}+v\frac{\partial T}{\partial y}=R_k\cdot\frac{1}{Pr\cdot Re}\left(\frac{\partial^2 T}{\partial x^2}+\frac{\partial^2 T}{\partial y^2}\right) \tag{4}$$

where x and y are the horizontal and vertical coordinates; u and v are the local dimensionless average velocity (Darcy velocity); T is the dimensionless average temperature; ε is the porosity; p_f is the intrinsic average pressure; R_k is the ratio of thermal conductivity in porous and fluid regions; Pr is the Prandtl number of the fluid; Da is the Darcy number; and Re is the Reynolds number. In the momentum equations (2) and (3), the second, the third and fourth terms on the right-hand side are called Darcy, Forchheimer and Brinkman terms, respectively.

The non-dimensional parameters are defined as follows:

$$\begin{aligned} R_k&=\frac{k_{\text{eff}}}{k_f}, \quad Pr=\frac{\mu}{\rho\alpha}\\ Da&=\frac{K}{H^2}, \quad Re=\frac{\mathrm{U}_{\text{av}}H\rho}{\mu}\end{aligned} \tag{5}$$

where H is the channel height; ρ is the fluid density; μ is the fluid kinematic viscosity; K is the permeability; α is the fluid thermal diffusivity; k_f is the fluid thermal conductivity; and k_{eff} is effective thermal conductivity of porous media.

For the homogeneous fluid part, the governing equations are

Continuity equation:

$$\frac{\partial u}{\partial x}+\frac{\partial v}{\partial x}=0 \tag{6}$$

X-momentum equation:

$$u\frac{\partial u}{\partial x}+v\frac{\partial u}{\partial y}=-\frac{\partial p}{\partial x}+\frac{1}{Re}\cdot\left(\frac{\partial^2 u}{\partial x^2}+\frac{\partial^2 u}{\partial y^2}\right) \tag{7}$$

Y-momentum equation:

$$u\frac{\partial v}{\partial x}+v\frac{\partial v}{\partial y}=-\frac{\partial p}{\partial y}+\frac{1}{Re}\cdot\left(\frac{\partial^2 v}{\partial x^2}+\frac{\partial^2 v}{\partial y^2}\right) \tag{8}$$

Energy equation:

$$u\frac{\partial T}{\partial x}+v\frac{\partial T}{\partial y}=\frac{1}{Pr\cdot Re}\left(\frac{\partial^2 T}{\partial x^2}+\frac{\partial^2 T}{\partial y^2}\right) \tag{9}$$

At the interface between the homogeneous fluid and porous medium regions, additional boundary conditions must be applied to couple the flows in the two domains. The boundary conditions include flow and heat transfer.

DOI: 10.1002/fld

For flow interfacial condition, the stress jump condition of Ochoa-Tapia and Whitaker [16] is applied:

$$\frac{1}{\varepsilon}\frac{\partial u_t}{\partial n}\bigg|_{\text{porous}} - \frac{\partial u_t}{\partial n}\bigg|_{\text{fluid}} = \beta\frac{1}{\sqrt{Da}}u_t\bigg|_{\text{interface}} + \beta_1 \cdot Re \cdot u_t^2 \tag{10}$$

where in the porous medium region, u_t is the Darcy velocity component parallel to the interface aligned with the direction t and normal to the direction n; in the homogeneous fluid region u_t is the fluid velocity component parallel to the interface; and β and β_1 are adjustable parameters which account for the stress jump at the interface. Considering the work done and reviewed before by Ochoa-Tapia and Whitaker [13, 16], for the purpose of demonstrating the implementation of the present formulation, both β and β_1 are varied in the range -1.0 to $+1.0$ in the present study.

In addition to Equation (10), the continuity of velocity and normal stress prevailing at the interface is given by

$$\mathbf{u}|_{\text{fluid}} = \mathbf{u}|_{\text{porous}} = \mathbf{v}_{\text{interface}} \tag{11}$$

$$\frac{1}{\varepsilon}\frac{\partial u_n}{\partial n}\bigg|_{\text{porous}} - \frac{\partial u_n}{\partial n}\bigg|_{\text{fluid}} = 0 \tag{12}$$

where in the porous medium region, u_n is the Darcy velocity component normal to the interface; and in the homogeneous fluid region, u_n is the fluid velocity component normal to the interface.

For heat transfer interfacial condition, continuities of temperature and heat flux are implemented here [8, 10, 11, 17–19, 31],

$$T|_{\text{fluid}} = T|_{\text{porous}} = T_{\text{interface}} \tag{13}$$

$$R_k \frac{\partial T}{\partial n}\bigg|_{\text{porous}} = \frac{\partial T}{\partial n}\bigg|_{\text{fluid}} \tag{14}$$

By combining with the appropriate boundary conditions of the composite regions, Equations (1)–(14) can be used to simulate the flow and heat transfer in a system composed of a porous medium and a homogeneous fluid.

The local and average Nusselt number and frictional loss [6, 7] are defined as

$$Nu = \frac{qH}{(T_w - T_{\text{i}})k_f} \tag{15}$$

$$Nu_{\text{av}} = \frac{1}{L}\int_l Nu\,\mathrm{d}x \tag{16}$$

$$h_l = \left(\frac{\bar{p}_{\text{i}}}{\rho_f} + \alpha_{\text{i}}\frac{U_{\text{i}}^2}{2}\right) - \left(\frac{\bar{p}_{\text{o}}}{\rho_f} + \alpha_{\text{o}}\frac{U_{\text{o}}^2}{2}\right) \tag{17}$$

where $\bar{p}_{\text{i}}$ and $\bar{p}_{\text{o}}$ are the average inlet and outlet pressures, and α_{i} and α_{o} are the kinetic coefficients, defined as

$$\alpha_{\text{i,o}} = \frac{\int_{A_{\text{i,o}}} u^3\,\mathrm{d}A}{\left(\int_{A_{\text{i,o}}} u\,\mathrm{d}A\right)^3} \tag{18}$$

DOI: 10.1002/fld

3. DISCRETIZATION OF THE GOVERNING EQUATIONS

The discretization of the governing equations are similar with previous research by Yu *et al.* [28], and now presented in Appendix. It is based on body-fitted, non-orthogonal grids, and multi-block strategy. As the energy equations are similar to momentum equations, only the discretization procedure for momentum is given out. The procedures for velocity and temperature at the interface are described here.

Although the case of study is that with a flat interface, generalized tangential and normal coordinates and unit vectors have been used so that the method can be extended to non-flat interfaces. However, it should be noted that curvature effects at the interface are not rigorously considered in the original models on which the equations solved are based. Furthermore, in some cases, structured grid are difficult, even impossible, to construct for complex geometries. Therefore, in the present study, multi-block grid method is applied to provide a compromise between the simplicity and wide variety of solvers available for structured grids and an ability to handle complex geometries that unstructured grids allow. Figure 2 shows details of the interface between two different blocks. Two neighboring control volumes, lying in Blocks A and B, respectively, share the interface. The grids in two neighboring blocks match at the interface. The treatment for fluid–porous medium interface is shown here.

3.1. Interface treatment for velocity and pressure

Blocks A and B (Figure 2) represent fluid and porous medium, respectively. The velocity vector at the interface is given by $\mathbf{v}_{\text{interface}}$. It can be written in either the x–y or n–t coordinate systems as

$$\mathbf{v}_{\text{interface}} = u\mathbf{e}_x + v\mathbf{e}_y = u_n\mathbf{n} + u_t\mathbf{t} \tag{19}$$

where u and v are the components of $\mathbf{v}_{\text{interface}}$ in the x and y directions while u_n and u_t are the $\mathbf{v}_{\text{interface}}$ components along n and t directions, respectively. Also, the component u_t then can be written as

$$u_t = u\mathbf{e}_x \cdot \mathbf{t} + v\mathbf{e}_y \cdot \mathbf{t} \tag{20}$$

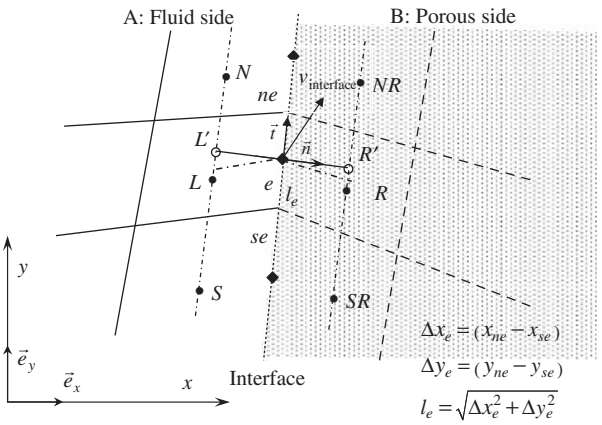

Figure 2. Interface between two blocks with matching grids.

DOI: 10.1002/fld

By combining Equations (10), (12) and (19):

$$\frac{1}{\varepsilon}\frac{\partial \mathbf{v}_{\text{interface}}}{\partial n}\bigg|_{\text{porous}} - \frac{\partial \mathbf{v}_{\text{interface}}}{\partial n}\bigg|_{\text{fluid}} = \beta\frac{1}{\sqrt{Da}}u_t\mathbf{t} + \beta_1 \cdot Re \cdot u_t^2\mathbf{t} \tag{21}$$

The unit vector ($\mathbf{t}$) parallel to the interface (Figure 2) is calculated from

$$\mathbf{t} = \frac{(x_{ne} - x_{se})\mathbf{e}_x + (y_{ne} - y_{se})\mathbf{e}_y}{\sqrt{(x_{ne} - x_{se})^2 + (y_{ne} - y_{se})^2}} = \frac{\Delta x_e \mathbf{e}_x + \Delta y_e \mathbf{e}_y}{l_e} \tag{22}$$

By substituting the components of $\mathbf{v}_{\text{interface}}$ in the x and y directions, Equation (21) becomes

$$\frac{1}{\varepsilon}\frac{\partial u}{\partial n}\bigg|_{\text{porous}} - \frac{\partial u}{\partial n}\bigg|_{\text{fluid}} = \beta\frac{1}{\sqrt{Da}}\frac{u\Delta x_e\Delta x_e + v\Delta y_e\Delta x_e}{l_e^2} + \beta_1 \cdot Re \cdot \frac{\Delta x_e(u\Delta x_e + v\Delta y_e)^2}{l_e^3} \tag{23}$$

$$\frac{1}{\varepsilon}\frac{\partial v}{\partial n}\bigg|_{\text{porous}} - \frac{\partial v}{\partial n}\bigg|_{\text{fluid}} = \beta\frac{1}{\sqrt{Da}}\frac{u\Delta x_e\Delta y_e + v\Delta y_e\Delta y_e}{l_e^2} + \beta_1 \cdot Re \cdot \frac{\Delta y_e(u\Delta x_e + v\Delta y_e)^2}{l_e^3} \tag{24}$$

The derivatives at the interface are calculated from the values at auxiliary nodes L' and R'; these nodes lie at the intersection of the cell face normal n and straight lines connecting nodes L and N or R and NR, respectively, as shown in Figure 2. The normal gradients at the interface can be calculated by using the first-order difference approximation:

$$\frac{\partial u}{\partial n}\bigg|_{\text{porous}} = \frac{u|_{R'} - u|_e}{L_{eR'}}, \quad \frac{\partial v}{\partial n}\bigg|_{\text{porous}} = \frac{v|_{R'} - v|_e}{L_{eR'}} \tag{25}$$

$$\frac{\partial u}{\partial n}\bigg|_{\text{fluid}} = \frac{u|_e - u|_{L'}}{L_{L'e}}, \quad \frac{\partial v}{\partial n}\bigg|_{\text{fluid}} = \frac{v|_e - v|_{L'}}{L_{L'e}} \tag{26}$$

The Cartesian velocity components at L' and R' can be calculated by using bilinear interpolation or by using the gradient at the control volume center:

$$u|_{L'} = u|_L + (\text{grad u})_L \cdot \mathbf{L'L} \tag{27}$$

To obtain higher-order approximation of the derivatives, the velocity components at more auxiliary nodes may be needed. Alternatively, the shape functions may be used, which produces a kind of combined finite element/finite volume method for calculating the higher-order approximations.

By using Equations (23)–(27) and explicitly calculating the terms at the right-hand sides of Equations (23) and (24), the Cartesian velocity components u and v at the interface are obtained. Then, the convective fluxes at the interface can be calculated. The diffusive fluxes are calculated from Equations (25)–(27). Then, the coefficients A_L and A_R can be obtained.

To close the algebra equation system, the pressure at the interface must be determined. For a single-domain approach, the velocity and pressure at the interface are coupled automatically, as the control volumes there are treated like those in the fluid or porous parts. However, with the present model, the pressure gradient at the interface may not be continuous due to the rather large Darcy and Forchheimer terms (Equation (2)), which may result in a rapid pressure drop at the porous side [26]. This discontinuity of the pressure gradient becomes more severe at higher Reynolds number and lower Darcy number. Thus, it requires special treatment to estimate the interface pressure from

DOI: 10.1002/fld

that of the vicinities at both sides. A simplistic pressure estimation may give unrealistic, oscillatory velocity profile. The coupling issue of pressure–velocity at the interface was described in a recent paper by Betchen *et al*. [26], who proposed a solution that enables stable calculations. The pressure is extrapolated in the fluid side to a location at a smaller distance near the interface. From this location, a momentum balance is then used to estimate the interface pressure. This estimate is then averaged with the pressure extrapolated from the porous side to obtain the interface pressure. In the present paper, a less complex treatment was adopted. Extrapolations from the fluid and porous sides give two different estimates of the interface pressure. The average of the two estimates is used as the interface pressure. A small number of iterations are required for accuracy.

3.2. Interface treatment for temperature

The heat transfer interface conditions are defined by Equations (13) and (14). Following the discretization procedure for the velocity above, the discretized equations at the interface are

$$R_k \left.\frac{\partial T}{\partial n}\right|_{\text{porous}} - \left.\frac{\partial T}{\partial n}\right|_{\text{fluid}} = 0 \tag{28}$$

$$\left.\frac{\partial T}{\partial n}\right|_{\text{porous}} = \frac{T|_{R'} - T|_e}{L_{eR'}} \tag{29}$$

$$\left.\frac{\partial T}{\partial n}\right|_{\text{fluid}} = \frac{T|_e - T|_{L'}}{L_{L'e}} \tag{30}$$

$$T|_{L'} = T|_L + (\text{grad}\, T)_L \cdot \mathbf{L}'\mathbf{L} \tag{31}$$

The temperature values at the interface can be obtained. The coefficients A_L and A_R for the energy equations can be used for the discretization along the interface control volume.

4. RESULTS AND DISCUSSION

In the present study, non-uniform, body-fitted and orthogonal meshes are employed, in which the density of meshes over the step back is larger than those in areas far downstream. The initial conditions for the computation were either a uniform flow at the inlet or the results of a previous calculation, often at different Reynolds numbers, Darcy numbers or porosity values. The divergence criteria are set as follows:

$$\sum|\varphi_{i,j}^{m+1} - \varphi_{i,j}^{m}| \Big/ \sum\varphi_{i,j}^{m+1} \leqslant \varepsilon \tag{32}$$

where $\varepsilon = 10^{-6}$. For simplicity, the ratio of the effective thermal conductivity of porous medium to fluid conductivity, R_k is set to be 1; the heat transfer would be more enhanced if the ratio is larger. The Prandtl number is set as $Pr = 0.72$, which is the value for air.

To validate the present computational code, Figure 3 compares the results for $Re = 800$ with those in benchmark studies, and there is good agreement with them as shown. Considering the computational cost and accuracy, the grid independency survey (details not given here) shows that a total 380×100 mesh, for both porous and fluid domains, is adequate.

DOI: 10.1002/fld

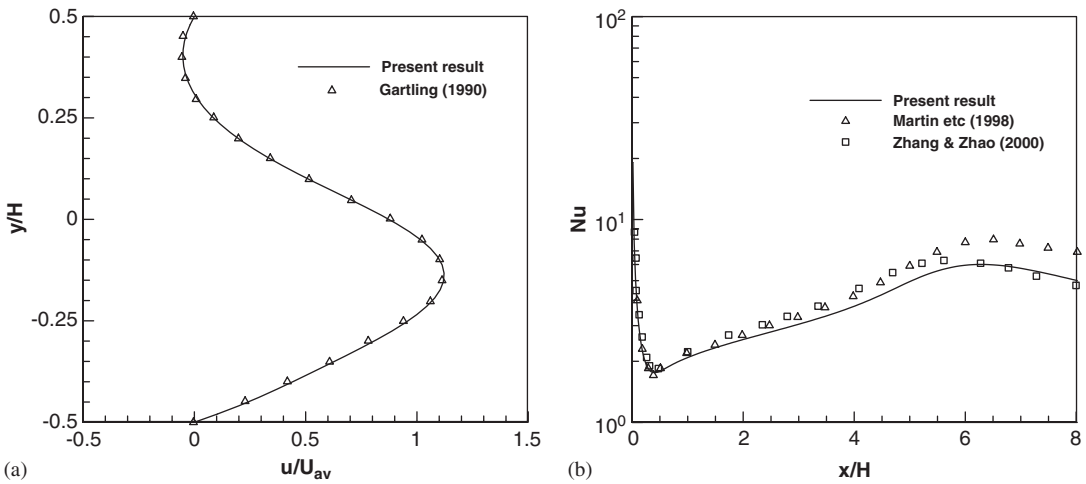

Figure 3. Forced convection past backward-facing step at $Re = 800$: (a) streamwise velocity profile at $x/H = 7$; and (b) lower wall Nusselt number *versus* axial location.

Figure 4 shows the stream contours of the flow for different Reynolds numbers from 10 to 800, at $Da = 10^{-2}$. It is observed that increasing the Reynolds number would increase the recirculation length, which is the distance from the back of the step to the vortex reattachment point. The flow field affects the heat transfer and this is shown in Figure 5 for the same Darcy number, in the form of axial distribution of lower wall Nusselt number. In the recirculation region, the heat transfer is first reduced. Then, it increases toward the attachment point, after which the Nusselt number gradually decreases toward the fully developed state. However, for low $Re = 10$, the recirculation region is so small that it does not cause much effect on the Nusselt number which shows a decrease with distance from the step. Higher Reynolds number gives higher Nusselt number as expected.

When the Darcy number is small, $Da = 10^{-4}$ (details not shown here), the flow after the step is different as there is no recirculation region even with $Re = 800$. There is no flow separation due to the small porous flow. The lower wall Nusselt number keep decreasing (Figure 6) with distance from the step. As Re increases to 800, the main heat transfer is convection. In the following computation, to study mainly the convective mode, the Re is set to 800.

The Darcy number effect is shown in Figure 7, with the same parameters as given in Zhang and Zhao [6], for the flow field at $Re = 800$. When the insert has high permeability, the recirculation length is still long (Figure 7(a)). With a lower permeability ($Da = 10^{-3}$ in Figure 7(b)), the insert breaks up the recirculation region into a small vortex in the region porous and a recirculation region in the fluid domain. With even lower Darcy number ($Da = 10^{-4}$ and 10^{-5} in Figures 7(c) and (d), respectively) the recirculation has disappeared. The effect on heat transfer is shown in Figure 8. Note that the scale is larger for ease of comparison later with results of Zhang and Zhao [6]. In the region downstream of the step, there is pronounced heat-transfer enhancement with lower Darcy numbers (high Nusselt number at $Da = 10^{-4}$). There is enhanced heat transfer due to elimination of the recirculation region. After the recirculation region has been suppressed, there is no further

DOI: 10.1002/fld

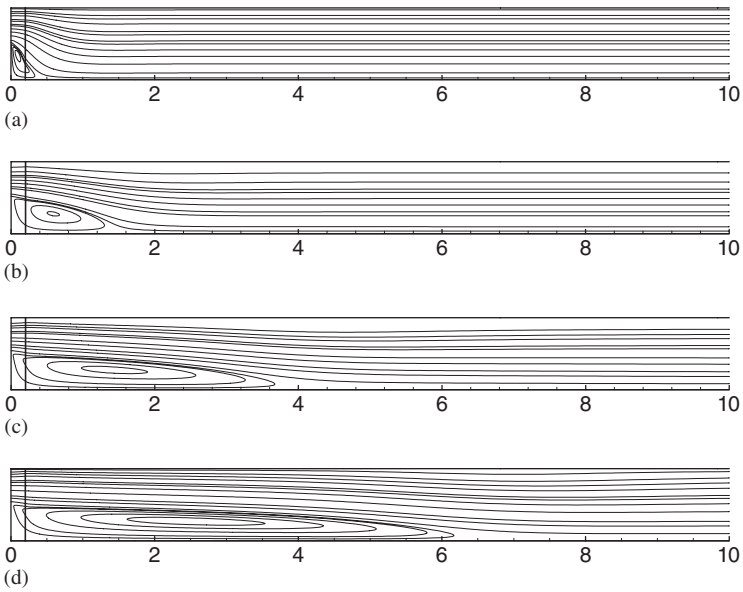

Figure 4. Streamline plots at Darcy number $Da = 10^{-2}$, inset length $a/H = 0.2$, porosity $\varepsilon = 0.4$, jump parameters $\beta = 0$ and $\beta_1 = 0$: (a) $Re = 10$; (b) $Re = 100$; (c) $Re = 400$; and (d) $Re = 800$.

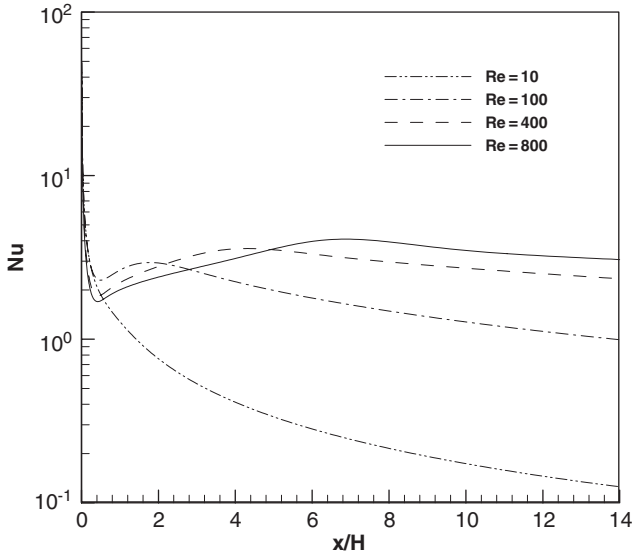

Figure 5. Axial distribution of lower wall Nusselt number at $Da = 10^{-2}$, $a/H = 0.2$, $\varepsilon = 0.4$, $\beta = 0$, and $\beta_1 = 0$.

enhancement of heat transfer when Darcy number is lowered to 10^{-5}; the Nusselt number drops due to lower convection in the porous insert. So for this $Re = 800$, there is an optimal Da between 10^{-4} and 10^{-5}.

DOI: 10.1002/fld

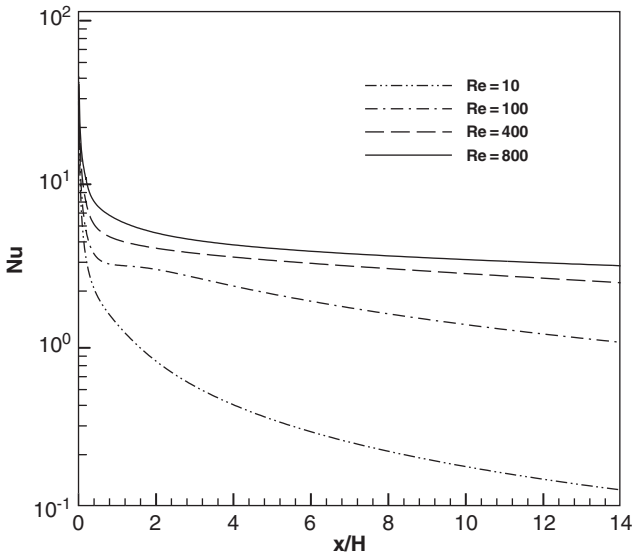

Figure 6. Axial distribution of lower wall Nusselt number at $Da = 10^{-4}$, $a/H = 0.2$, $\varepsilon = 0.4$, $\beta = 0$, and $\beta_1 = 0$.

A comparison with the one-domain results of Zhang and Zhao [6] is also shown in Figure 8. The main difference in the two methods is the treatment of the interface pressure and velocity as discussed in Section 3.1. Note that the present stress jump parameters were set to zero to permit a comparison with the one-domain model. As compared with the one-domain results, there is little discrepancy of the Nusselt numbers in the regions inside the porous insert and far downstream. Some discrepancies are found in the region just downstream of the porous insert. However, the discrepancies are small for $Da = 10^{-4}$ (see Figure 8). At this small Da, there is no recirculation region (Figure 7) which may explain why the interface treatment seems to have less effect. The unseparated gross-flow downstream of the porous inserts, being mainly determined by the channel height, would be relatively less sensitive to the interface pressure. At larger Darcy numbers (10^{-2} and 10^{-3}), the discrepancies are significant which is attributed to the presence of the recirculation regions (see streamline Figures 7(a) and (b)). It is noted that the recirculation lengths computed here are longer than those of Zhang and Zhao [6]. The comparison indicates that the interface pressure has greater effects on the downstream flow, and hence the local Nusselt number, when there is a recirculation region. Thus, a careful treatment of the interface pressure would be advantageous when the flow pattern is complex.

Figure 9 shows the effect of the porous insert length on the flow field with $Da = 10^{-2}$. With an insert length of zero or small, there are two recirculation regions. A longer insert length of $a/H = 0.2$ suppresses the upper recirculation region. Longer insert also reduces the length of the lower recirculation region. However, there is little difference in Nusselt numbers (details not shown here) as the insert length does not suppress the bottom recirculation. It is not suppressed, even with a longer insert, because there is insufficient flow resistance with a large Darcy number.

Figure 10 shows the effect of the porous insert length on the flow field with a smaller $Da = 10^{-4}$. With longer insert, the recirculation regions are completely suppressed (Figure 10(c) and (d)).

DOI: 10.1002/fld

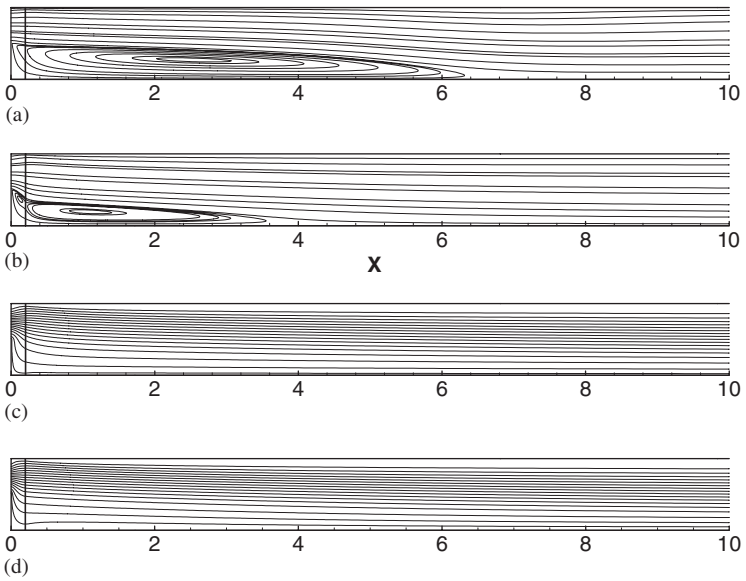

Figure 7. Streamline plots at $Re = 800$, $a/H = 0.2$, $\varepsilon = 0.99$, $\beta = 0$, and $\beta_1 = 0$ with various Darcy numbers: (a) $Da = 10^{-2}$; (b) $Da = 10^{-3}$; (c) $Da = 10^{-4}$; and (d) $Da = 10^{-5}$.

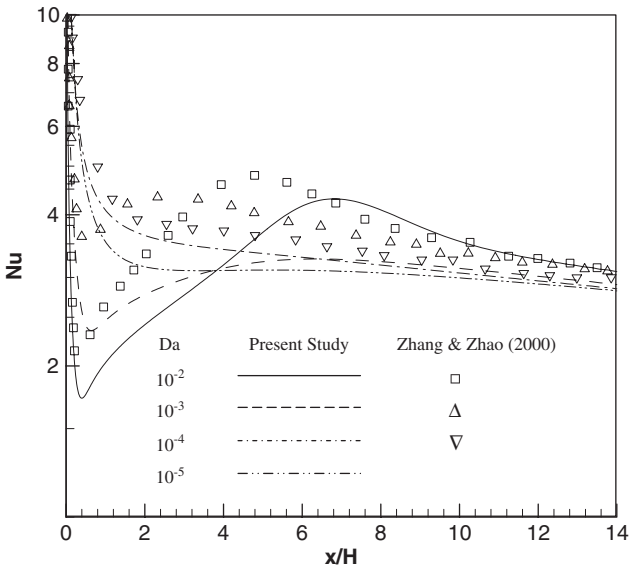

Figure 8. Axial distribution of lower wall Nusselt number at $Re = 800$, $a/H = 0.2$, $\varepsilon = 0.99$, $\beta = 0$, and $\beta_1 = 0$ with various Darcy numbers.

Figure 11 shows the corresponding axial distribution of lower wall Nusselt number. The longer inserts give more enhanced heat transfer behind the step due to the elimination of recirculation region.

DOI: 10.1002/fld

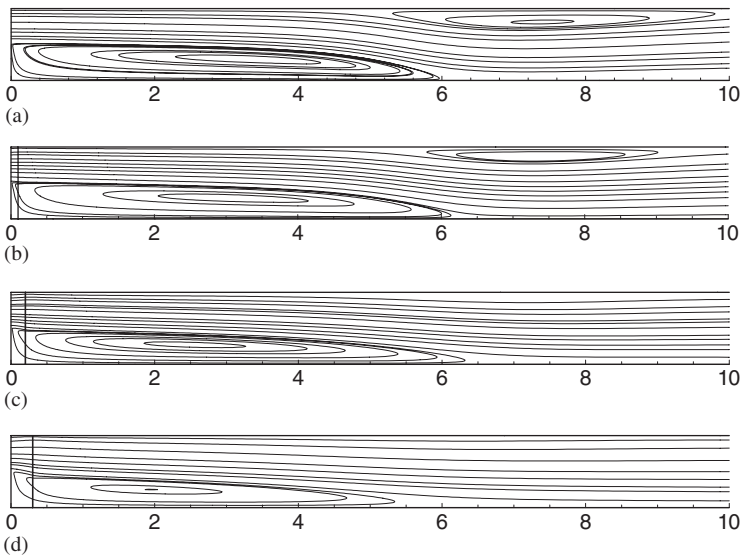

Figure 9. Streamline plots at $Re = 800$, $Da = 10^{-2}$, $\varepsilon = 0.4$, $\beta = 0$, and $\beta_1 = 0$ with various insert lengths: (a) $a/H = 0.0$; (b) $a/H = 0.1$; (c) $a/H = 0.2$; and (d) $a/H = 0.3$.

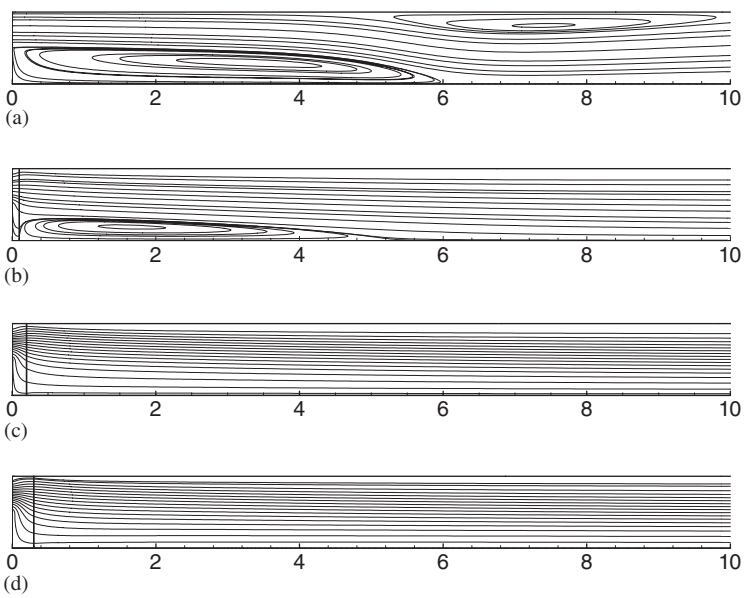

Figure 10. Streamline plots at $Re = 800$, $Da = 10^{-4}$, $\varepsilon = 0.4$, $\beta = 0$, and $\beta_1 = 0$ with various insert lengths: (a) $a/H = 0.0$; (b) $a/H = 0.1$; (c) $a/H = 0.2$; and (d) $a/H = 0.3$.

Figure 12 gives out the porosity effect on the axial distribution of lower wall Nusselt number with $Da = 10^{-4}$. A smaller porosity gives higher Nusselt number behind the step, as expected. However, the porosity effect is rather small.

DOI: 10.1002/fld

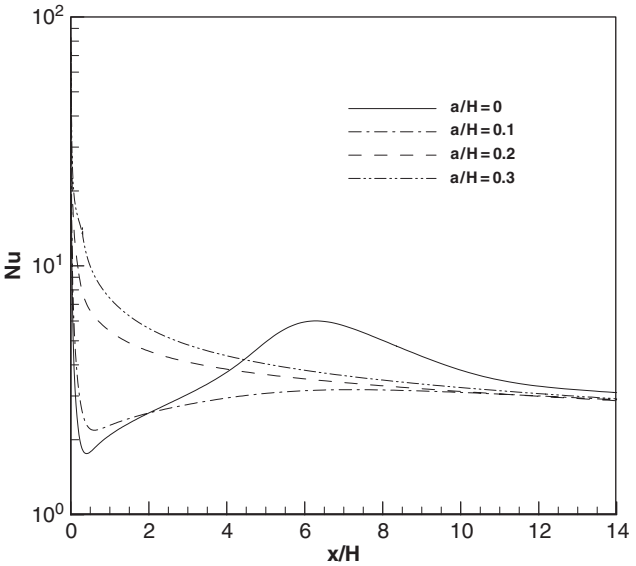

Figure 11. Axial distribution of lower wall Nusselt number for $\varepsilon = 0.4$, $Re = 800$, $Da = 10^{-4}$, $\beta = 0$, and $\beta_1 = 0$.

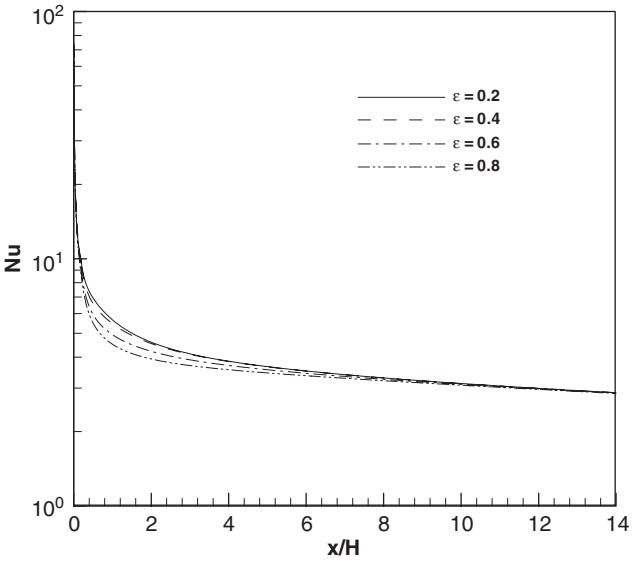

Figure 12. Axial distribution of lower wall Nusselt number for $a/H = 0.2$, $Re = 800$, $Da = 10^{-4}$, $\beta = 0$, and $\beta_1 = 0$.

Figure 13(a) and (b) shows velocity profiles behind the step ($x/H = 0.5$) for a short and long inserts, respectively. With a short insert (Figure 13(a)), there is negative or small velocity near the lower wall due to the recirculation regions (see Figure 9(b) and 10(b)). With a long insert (Figure

DOI: 10.1002/fld

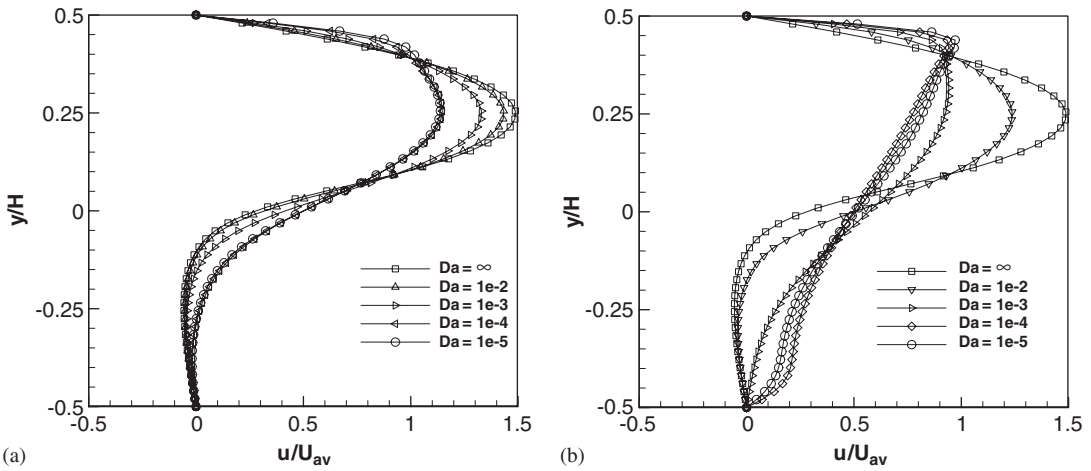

Figure 13. Streamwise velocity profiles at $x/H = 0.5$, with $Re = 800$, $Da = 10^{-2}$, $\beta = 0$, and $\beta_1 = 0$: (a) $a/H = 0.1$; and (b) $a/H = 0.3$.

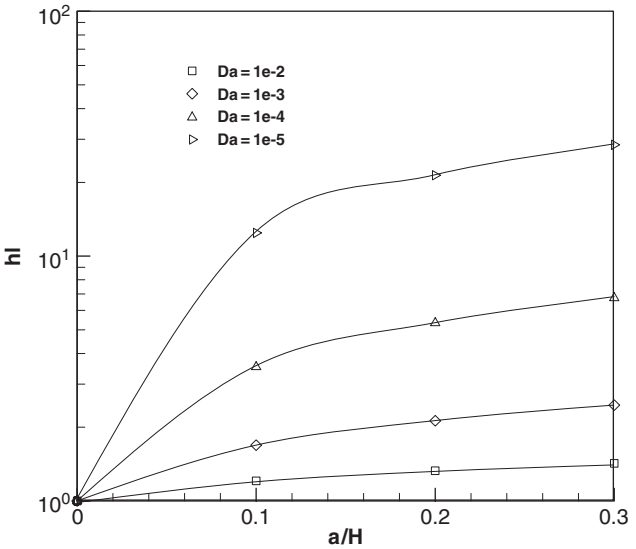

Figure 14. Dimensionless channel head loss, with $Re = 800$, $\varepsilon = 0.4$, $\beta = 0$, and $\beta_1 = 0$.

13(b)), the velocity profiles are greatly affected by the Darcy number. With large $Da \geqslant 10^{-2}$, there is negative velocity near the lower wall due to the recirculation region (see Figure 9(d)). When Da decreases to $\leqslant 10^{-3}$, there is forward velocity near the bottom wall as the bottom recirculation region has been eliminated (see Figure 10(d) for $Da = 10^{-4}$). The velocity profiles explain the enhancement of the local heat convection in the bottom region behind the step. However, there is no additional enhancement below $Da = 10^{-4}$. Once the recirculation has been suppressed, a further decrease in the Darcy number to 10^{-5} will give lower velocity (compared with that of

DOI: 10.1002/fld

Table III. Average Nusselt number for lower wall with different stress jump parameters at $Re = 800$, $\varepsilon = 0.4$, $a/H = 0.2$.

Da	β	β_1	Nu_{av}	Da	β	β_1	Nu_{av}
10^{-2}	0	−1	3.276	10^{-4}	0	−1	3.855
	0	0	3.273		0	0	3.826
	0	1	3.273		0	1	3.785
	−1	0	3.272		−1	0	3.844
	0	0	3.273		0	0	3.826
	1	0	3.275		1	0	3.807
	1	1	3.275		1	1	3.741
	−1	−1	3.273		−1	−1	3.902

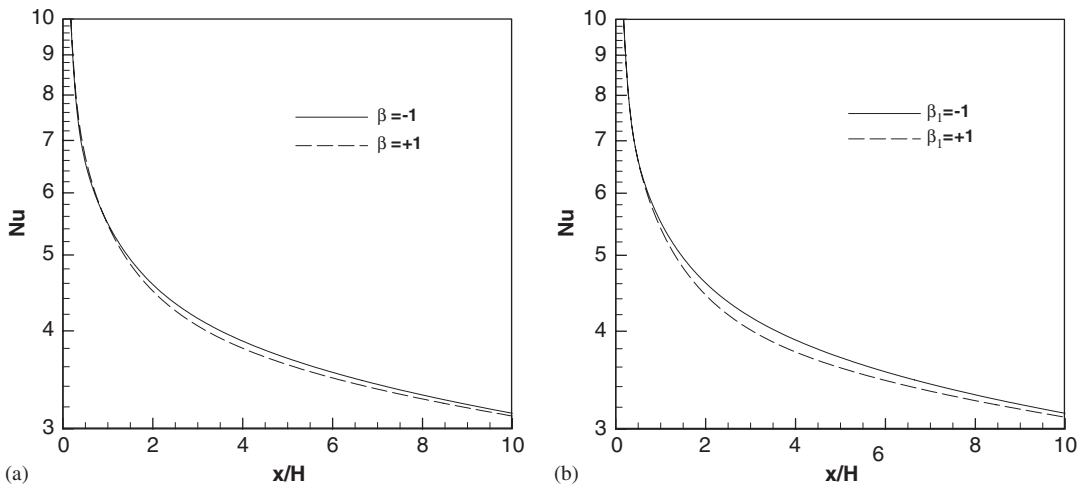

Figure 15. Effect of stress jump parameters on the local Nusselt number with $a/H = 0.2$, $Re = 800$, $\varepsilon = 0.4$, and $Da = 10^{-4}$: (a) β effect with $\beta_1 = 0$ and (b) β_1 effect with $\beta = 0$.

$Da = 10^{-4}$ as shown in Figure 13(b)). Thus, there is an optimal Darcy number to achieve enhanced heat transfer at the lower wall as mentioned earlier (shown in Figure 8).

In Figure 14, the dimensionless channel head loss (normalized by that with no porous insert) is shown as a function of insert length and Darcy number. The head loss is higher with longer insert length or smaller Darcy number, as expected. To achieve optimal enhancement of heat transfer, it is necessary to avoid excessive frictional losses. Thus, a combination of medium Darcy number and insert length is preferred.

The stress jump parameters were varied from −1 to +1 and its effect on the average lower wall Nusselt number is presented in Table III for $Re = 800$. It can be observed that for the larger Darcy number $Da = 10^{-2}$, there is little effect; the insert is too porous to affect the recirculation region as discussed earlier. For the smaller Darcy number $Da = 10^{-4}$, the difference is more noticeable but still not large, about 4% when both β and β_1 are varied from −1 to 1. It is not surprising that the jump coefficients have little effect on average values like the wall Nusselt number presented

DOI: 10.1002/fld

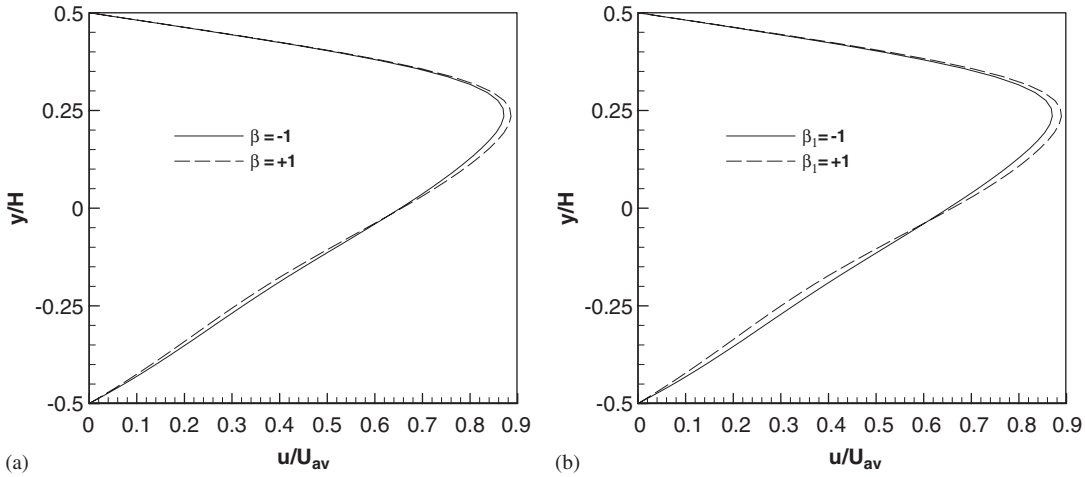

Figure 16. Effect of stress jump parameters on the velocity profile at $x/H = 3.0$ with $a/H = 0.2$, $Re = 800$, $\varepsilon = 0.4$, and $Da = 10^{-4}$: (a) β effect with $\beta_1 = 0$ and (b) β_1 effect with $\beta = 0$.

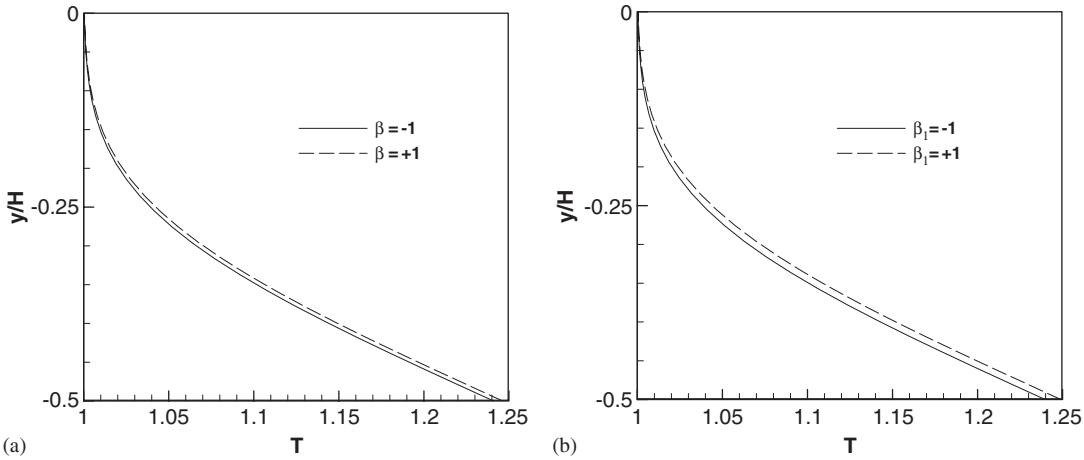

Figure 17. Effect of stress jump parameters on the temperature profile at $x/H = 3.0$ with $a/H = 0.2$, $Re = 800$, $\varepsilon = 0.4$, $Da = 10^{-4}$: (a) β effect with $\beta_1 = 0$ and (b) β_1 effect with $\beta = 0$.

in Table III. In the literature, it is possible to find studies [32] which show that even the type of formulation has almost no effect on global coefficients.

The importance of a numerical method that considers properly the effect of the jump coefficients or the formulation of the boundary conditions should be assessed by analyzing local variable predictions in the neighborhood of the interface fluid–porous medium. The effect of the stress jump parameters on the local Nusselt number is shown in Figure 15. Their effects on the local velocity and temperature profiles at $x/H = 3.0$ are shown, respectively, in Figures 16 and 17. It is noted that there are some effects of β and β_1 when they are varied from -1 to $+1$. Positive

DOI: 10.1002/fld

parameters give a larger peak velocity and smaller velocity near the wall. Thus, the temperatures are smaller there and hence the Nusselt numbers are larger.

The effect of stress jump parameters is small in the present case because the dominant flow direction is near normal to the interface. In parallel flow past a porous–fluid interface [27], in which the porous medium partially fills the channel, it was found that the velocity profile was very sensitive to the stress parameters. It is expected that the stress parameters will have greater effect on the heat transfer, if the porous insert was designed to partially fill the channel in order to avoid high friction losses.

5. CONCLUSION

A numerical method was implemented to treat the forced convection in porous and fluid domains coupled at the interface by stress jump for velocity. The continuities of temperature and heat flux were imposed. The method was based on finite volume method, with body-fitted, non-orthogonal grids, and multi-block strategy. The generalized Darcy–Brinkman–Forchheimer extended model was used to describe the flow in the porous region, considering the inertia, convective, and viscous effects.

The two-dimensional forced convection through a porous insert behind a backward-facing step was simulated numerically. The stress jump condition, including viscous and inertia effects, was used for the interface between the porous and fluid media. Results are presented with flow configurations for different Darcy numbers, 10^{-2} to 10^{-5}, porosities from 0.2 to 0.8, and Reynolds numbers from 10 to 800, and ratio of insert length to channel height from 0.1 to 0.3. The Darcy number, Reynolds number and insert length influence the recirculation regions and hence the heat transfer, but the porosity effect is small. To achieve optimal heat transfer effect, without excessive frictional loss, it is preferable to use a medium insert length with flow at medium Darcy number and large Reynolds number.

The stress jump parameters have small effects on the average lower wall Nusselt number. For the smaller Darcy number $Da = 10^{-4}$, the difference in Nu is about 4%, when both β and β_1 are varied from -1 to 1. The effects are more discernible on the local velocity and temperature profiles. The stress parameters may have even more significant effects on the heat transfer if the dominant flow direction is nearly tangential to the interface, as in the case of a porous insert that partially fills the channel in order to avoid high friction losses.

The present work continues the previous study of Yu *et al.* [28], which treated the flow boundary condition at the interface between porous and homogeneous regions by imposing a shear stress jump with a continuity of normal stress. The thermal boundary conditions, as well as the discretization procedure for the energy equation, are added in the present paper, based on the continuity of temperature and heat flux. Such thermal boundary conditions, in previous numerical works [18, 24–26, 32], have been combined with continuity of shear and normal stresses together with slip or no-slip velocity boundary conditions. However, the present flow boundary conditions are a shear stress jump with a continuity of normal stress. It can address general problems of forced convection in porous and homogeneous fluid domains, in which the flow and thermal interfacial conditions need to be considered in detail. In addition, the present numerical implementation is suitable for complex geometries, as it is based on the finite volume method using body-fitted grids and multi-block technique.

DOI: 10.1002/fld

From the numerical method point of view, the present work contributes a numerical implementation that can deal with the flow-thermal boundary-conditions at the interface between porous medium and homogeneous fluid domains. The method was applied to the physical situation of a backward facing step with porous insert that typifies convective heat transfer in a fluid–porous heterogeneous region. The main contribution relies on the numerical technique not in the development of the stress jump flow model which was derived by Ochoa-Tapia and Whitaker [16].

APPENDIX: DISCRETIZATION OF THE GOVERNING EQUATIONS

A.1. Homogeneous fluid region

A typical control volume is shown in Figure A1. For a general dependent variable φ, a final discrete form over the control volume can be written as

$$F_e + F_w + F_n + F_s = S \tag{A1}$$

where F_e, F_w, F_n and F_s are the overall fluxes (including both convection and diffusion) of φ at faces e, w, n, s, which denote east, west, north, and south of the control volume; and S is the source term. The detailed numerical methodology for obtaining the convective flux (F_e^c, F_w^c, F_n^c, and F_s^c) and diffusive flux (F_e^d, F_w^d, F_n^d, and F_s^d) are given in Ferziger and Perić [33].

With the midpoint rule approximation, the convective flux at face east can be calculated as:

$$F_e^c = \int_{S_e} \varphi \mathbf{u} \cdot \mathbf{n} \, \mathrm{d}S \approx m_e \varphi_e \tag{A2}$$

where m_e is the dimensionless mass flux cross the surface e; S_e is the surface area of face e; and φ_e is the value of φ at the center of the cell face. m_e and S_e can be calculated as

$$m_e = (S^x u + S^y v)_e, \quad S_e = \sqrt{(S_e^x)^2 + (S_e^y)^2} \tag{A3}$$

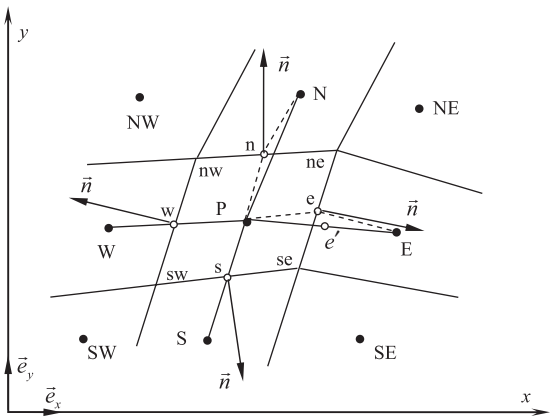

Figure A1. Interface between two blocks with matching grids.

DOI: 10.1002/fld

where u and v are the velocity components in the x and y directions; S^x and S^y are the surface vector components.

To avoid the non-orthogonal effect, the midpoint rule with the deferred correction term [34] applied to the integrated diffusive flux is given by

$$F_e^d = \frac{1}{Re}\left(\frac{\partial\varphi}{\partial n}\right)_e S_e = \frac{1}{Re}S_e\left(\frac{\partial\varphi}{\partial\xi}\right)_e + \frac{1}{Re}S_e\left[\overline{\left(\frac{\partial\varphi}{\partial n}\right)_e} - \overline{\left(\frac{\partial\varphi}{\partial\xi}\right)_e}\right]^{\text{old}} \tag{A4}$$

If an implicit flux approximation of the term $(\partial\varphi/\partial\xi)_e$ is applied, the final expression of Equation (A4) then becomes

$$F_e^d = \frac{1}{Re}S_e\frac{\varphi_E - \varphi_P}{L_{PE}} + \frac{1}{Re}S_e\overline{(\text{grad}\,\varphi)_e}^{\text{old}} \cdot (\mathbf{n} - \mathbf{i}_\xi) \tag{A5}$$

where L_{PE} stands for the distance between P and E; $\mathbf{i}_\xi$ is the unit vector in the ξ-direction.

The different methods to approximate the value of ϕ and its derivative at the cell face result in different interpolation schemes. In the present study, the central difference scheme (CDS) is used. Then the cell-face values of the variables are approximated as

$$\varphi_e \approx \varphi_{e'} = \lambda_e\varphi_E + (1 - \lambda_e)\varphi_P \quad \text{for face } e \tag{A6}$$

where the interpolation factor λ_e is defined as

$$\lambda_e = \frac{|\mathbf{r}_e - \mathbf{r}_P|}{|\mathbf{r}_e - \mathbf{r}_P| + |\mathbf{r}_E - \mathbf{r}_e|} \tag{A7}$$

where $\mathbf{r}_e$ is the position vector.

Equation (A6) is a second-order approximation at the location e' on the straight line connecting nodes P and E (Figure A1). If the cell-face center e does not coincide with the location e', a correction term needs to be added in Equation (A6) to restore the second-order accuracy, which can be expressed as follows:

$$\varphi_e \approx \varphi_{e'} + (\text{grad}\,\varphi)_{e'} \cdot (\mathbf{r}_e - \mathbf{r}_{e'}) \tag{A8}$$

To obtain the deferred derivatives at the cell face, they are calculated first at the control volume centers and then interpolated to the cell faces. By using the Gauss theorem, the derivative at the CV centers can be approximated by the average value over the cell:

$$\left(\frac{\partial\varphi}{\partial x_i}\right)_P \approx \frac{\int_\Omega(\partial\varphi/\partial x_i)\,\mathrm{d}\Omega}{\Delta\Omega} = \int_S \varphi\mathbf{i}_i \cdot \mathbf{n}\,\mathrm{d}S \approx \sum_c \varphi_c S_c^i, \quad c = e, n, w, s \tag{A9}$$

Then, the cell-center derivatives can also be interpolated to the cell-face centers using the same interpolation as that described by Equations (A6)–(A8).

The volume integral of the source term is

$$Q_\varphi = \int_\Omega S_\varphi\,\mathrm{d}\Omega \approx S_\varphi\Delta\Omega \tag{A10}$$

where Ω is the cell volume.

DOI: 10.1002/fld

The momentum equations contain a contribution from the pressure. The volume integral of the pressure gradient term in the u-momentum equation can be obtained by

$$Q^p_{u,P} = \int_\Omega -\left(\frac{\partial p}{\partial x}\right)_P \mathrm{d}\Omega \approx -\left(\frac{\delta p}{\delta x}\right)_P \Delta\Omega \tag{A11}$$

Then, the final discrete form of the u-momentum equation is

$$A^u_P u_P + \sum_l A^u_l u_l = Q^*_{u,P} - \left(\frac{\delta p}{\delta x}\right)_P \Delta\Omega \tag{A12}$$

where P is the index of an arbitrary node; the index l denotes the four neighboring points E, W, S, N; the coefficients A^φ_P, A^φ_E, A^φ_W, A^φ_N, A^φ_S are those of the resultant algebraic equations; and $Q^*_{u,P}$ is the integral of the source term contributed by other forces.

In the present study, SIMPLEC method [35] is applied to couple the velocity and pressure. To avoid oscillations in the pressure or velocity, the interpolation proposed by Rhie and Chow [36] is adopted:

$$u^m_e = \overline{(u^m)_e} - \Delta\Omega_e \overline{\left(\frac{1}{A^u_P + \sum_l A^u_l}\right)}_e \left[\left(\frac{\delta p}{\delta x}\right)_e - \overline{\left(\frac{\delta p}{\delta x}\right)}_e\right]^{m-1} \tag{A13}$$

where m is iteration step for each time level.

A.2. Porous medium region

Equations (1)–(3) recover the standard Navier–Stokes equations when the porosity approaches unity. Thus, the discretizing procedure for porous medium is similar to that for the homogeneous fluid as the two sets of governing equations are similar in form. The discretized diffusion flux is similar in form to Equation (A6). The convective flux at a cell face is similar in form to Equation (A2) except for a small change:

$$F^c_e = \frac{1}{\varepsilon}\int_{S_e} \frac{u}{\varepsilon}\mathbf{u}\cdot\mathbf{n}\,\mathrm{d}S \approx m_e u_e/\varepsilon^2_e \tag{A14}$$

The volume integral of the pressure gradient term (similar in form to Equation (A11)) is

$$Q^{p*}_{u,P} = \frac{1}{\varepsilon}\int_\Omega -\left(\frac{\partial(\varepsilon p^*)}{\partial x}\right)_P \mathrm{d}\Omega \approx -\frac{1}{\varepsilon_p}\left(\varepsilon\frac{\delta p}{\delta x}\right)_P \Delta\Omega \tag{A15}$$

For the Darcy term in Equations (2) and (3), the volume integral can be expressed as

$$Q^u_D = \int_\Omega -\left(\frac{1}{Da\cdot Re}u\right)_p \mathrm{d}\Omega = -\left(\frac{1}{Da\cdot Re}\right)_p \Delta\Omega\cdot u_p \tag{A16}$$

For the Forchheimer term, the volume integral is given by

$$Q^u_F = \int_\Omega -\left(\frac{1.75\cdot\sqrt{u^2+v^2}}{\sqrt{150}\cdot\sqrt{Da}\cdot\varepsilon^{3/2}}u\right)_p \mathrm{d}\Omega = -\left(\frac{1.75\cdot\sqrt{u^2+v^2}}{\sqrt{150}\cdot\sqrt{Da}\cdot\varepsilon^{3/2}}u\right)_p \Delta\Omega\cdot u_p \tag{A17}$$

It is convenient to treat the Darcy and Forchheimer terms as source terms. However, Equations (A16) and (A17) indicate that, after integrating, both terms become a product of Darcy

DOI: 10.1002/fld

velocity component and a coefficient. The two coefficients can be added into the coefficients of the algebraic equation A_p^u, which will accelerate the convergence rate.

The procedure to obtain the pressure correction equation is also similar to that for homogeneous fluid (Equation (A13)), except for a small change:

$$u_e^m = \overline{(u^m)_e} - \Delta\Omega_e \overline{\left(\frac{1}{A_P^u + \sum_l A_l^u}\right)_e} \left[\left(\frac{\delta(\varepsilon p^*)}{\delta x}\right)_e - \overline{\left(\frac{\delta(\varepsilon p^*)}{\delta x}\right)_e} \right]^{m-1} \tag{A18}$$

REFERENCES

1. Huang PC, Vafai K. Analysis of forced convection enhancement in a channel using porous blocks. *Journal of Thermophysics and Heat Transfer* 1994; **8**(3):563–573.
2. Vafai K, Huang PC. Analysis of heat transfer regulation and modification employing intermittently emplaced porous cavities. *Journal of Heat Transfer* (ASME) 1994; **116**:604–613.
3. Fu W-S, Huang H-C, Liou W-Y. Thermal enhancement in laminar channel flow with a porous block. *International Journal of Heat and Mass Transfer* 1996; **39**(10):2165–2175.
4. Abu-Hijleh B. Convection heat transfer from a laminar flow over a 2-D backward facing step with asymmetric and orthotropic porous floor segments. *Numerical Heat Transfer A* 1997; **31**:325–335.
5. Martin AR, Satiel C, Shyy W. Heat transfer enhancement with porous inserts in recirculating flow. *Journal of Heat Transfer* 1998; **120**:458–467.
6. Zhang B, Zhao Y. A numerical method for simulation of forced convection in a composite porous/fluid system. *International Journal of Heat and Fluid Flow* 2000; **21**:432–441.
7. Beavers GS, Joseph DD. Boundary conditions at a natural permeable wall. *Journal of Fluid Mechanis* 1967; **30**:197–207.
8. Neale G, Nader W. Practical significance of Brinkman's extension of Darcy's law: coupled parallel flows within a channel and a bounding porous medium. *Canadian Journal of Chemical Engineering* 1974; **52**:475–478.
9. Vafai K, Kim SJ. Fluid mechanics of the interface region between a porous medium and a fluid layer—an exact solution. *International Journal of Heat and Fluid Flow* 1990; **11**:254–256.
10. Vafai K, Thiyagaraja R. Analysis of flow and heat transfer at the interface region of a porous medium. *International Journal of Heat and Mass Transfer* 1987; **30**:1391–1405.
11. Kim SJ, Choi CY. Convective heat transfer in porous and overlying layers heated from below. *International Journal of Heat and Mass Transfer* 1996; **39**:319–329.
12. Ochoa-Tapia JA, Whitaker S. Momentum transfer at the boundary between a porous medium and a homogeneous fluid I: theoretical development. *International Journal of Heat and Mass Transfer* 1995; **38**:2635–2646.
13. Ochoa-Tapia JA, Whitaker S. Momentum transfer at the boundary between a porous medium and a homogeneous fluid II: comparison with experiment. *International Journal of Heat and Mass Transfer* 1995; **38**:2647–2655.
14. Goyeau B, Lhuillier D, Gobin D, Velarde MG. Momentum transport at a fluid–porous interface. *International Journal of Heat and Mass Transfer* 2003; **46**:4071–4081.
15. Chandesris M, Jamet D. Boundary conditions at a planar fluid–porous interface for a Poiseuille flow. *International Journal of Heat and Mass Transfer* 2006; **49**:2137–2150.
16. Ochoa-Tapia JA, Whitaker S. Momentum jump condition at the boundary between a porous medium and a homogeneous fluid: inertial effect. *Journal of Porous Media* 1998; **1**:201–217.
17. Ochoa-Tapia JA, Whitaker S. Heat transfer at the boundary between a porous medium and a homogeneous fluid. *International Journal of Heat and Mass Transfer* 1997; **40**:2691–2707.
18. Jang JY, Chen JL. Forced convection in a parallel plate channel partially filled with a high porosity medium. *International Communications in Heat and Mass Transfer* 1992; **19**:263–273.
19. Kuznetsov AV. Fluid mechanics and heat transfer in the interface region between a porous medium and a fluid layer: a boundary layer solution. *Journal of Porous Media* 1999; **2**(3):309–321.
20. Ochoa-Tapia JA, Whitaker S. Heat transfer at the boundary between a porous medium and a homogeneous fluid: the one-equation model. *Journal of Porous Media* 1998; **1**:31–46.
21. Sahraoui M, Kaviany M. Slip and no-slip temperature boundary conditions at the interface of porous, plain media: convection. *International Journal of Heat and Mass Transfer* 1994; **37**:1029–1044.

DOI: 10.1002/fld

22. Jue TC. Numerical analysis of vortex shedding behind a porous cylinder. *International Journal of Numerical Methods for Heat and Fluid Flow* 2004; **14**:649–663.
23. Silva RA, de Lemos MJS. Numerical analysis of the stress jump interface condition for laminar flow over a porous layer. *Numerical Heat Transfer A* 2003; **43**:603–617.
24. Costa VAF, Oliveira LA, Baliga BR, Sousa ACM. Simulation of coupled flows in adjacent porous and open domains using a control-volume finite-element method. *Numerical Heat Transfer A* 2004; **45**:675–697.
25. Gartling DK, Hickox CE, Givler RC. Simulation of coupled viscous and porous flow problems. *Computational Fluid Dynamics* 1996; **7**:23–48.
26. Betchen L, Straatman AG, Thompson BE. A nonequilibrium finite-volume model for conjugate fluid/porous/solid domains. *Numerical Heat Transfer A* 2006; **49**:543–565.
27. Alazmi B, Vafai K. Analysis of fluid flow and heat transfer interfacial conditions between a porous medium and a fluid layer. *International Journal of Heat and Mass Transfer* 2001; **44**:1735–1749.
28. Yu P, Lee TS, Zeng Y, Low HT. A numerical method for flows in porous and homogenous fluid domains coupled at the interface by stress jump. *International Journal for Numerical Methods in Fluids* 2007; **53**:1755–1775.
29. Hsu CT, Cheng P. Thermal dispersion in a porous medium. *International Journal of Heat and Mass Transfer* 1990; **33**:1587–1597.
30. Nithiarasu P, Seetharamu KN, Sundararajan T. Finite element modelling of flow, heat and mass transfer in fluid saturated porous media. *Archives of Computational Methods in Engineering* 2002; **9**:3–42.
31. Alazmi B, Vafai K. Analysis of fluid flow and heat transfer interfacial conditions between a porous medium and a fluid layer. *International Journal of Heat and Mass Transfer* 2001; **44**:1735–1749.
32. Valencia-Lopez JJ, Ochoa-Tapia JA. A study of buoyancy-driven flow in a confined fluid overlying a porous layer. *International Journal of Heat and Mass Transfer* 2001; **44**:4725–4736.
33. Ferziger JH, Perić M. *Computational Methods for Fluid Dynamics* (2nd edn). Springer: Berlin, 1999; 222–233.
34. Muzaferija S. Adaptive finite volume method for flow predictions using unstructured meshes and multigrid approach. *Ph.D. Thesis*, University of London, 1994.
35. van Doormal JP, Raithby GD. Enhancements of the SIMPLE method for predicting incompressible fluid flows. *Numerical Heat Transfer* 1984; **7**:147–163.
36. Rhie CM, Chow WL. Numerical study of the turbulent flow past an airfoil with trailing edge separation. *AIAA Journal* 1983; **21**:1525–1532.

DOI: 10.1002/fld